Published in final edited form as:
Neuroimage. 2014 February 15; 87: 287–296. doi:10.1016/j.neuroimage.2013.10.055.

Early anti-correlated BOLD signal changes of physiologic origin

Molly G. Bright[a,b,*], **Marta Bianciardi**[a,c], **Jacco A. de Zwart**[a], **Kevin Murphy**[b], and **Jeff H. Duyn**[a]

[a]Advanced MRI Section, LFMI, NINDS, National Institutes of Health, Bethesda, MD, USA

[b]Cardiff University Brain Research Imaging Centre (CUBRIC), School of Psychology, Cardiff University, Cardiff, UK

[c]Department of Radiology, Athinoula A. Martinos Center for Biomedical Imaging, Massachusetts General Hospital, Harvard Medical School, Boston, MA, USA

Abstract

Negative BOLD signals that are synchronous with resting state fluctuations have been observed in large vessels in the cortical sulci and surrounding the ventricles. In this study, we investigated the origin of these negative BOLD signals by applying a Cued Deep Breathing (CDB) task to create transient hypocapnia and a resultant global fMRI signal decrease. We hypothesized that a global stimulus would amplify the effect in large vessels and that using a global negative (vasoconstrictive) stimulus would test whether these voxels exhibit either inherently negative or simply anti-correlated BOLD responses. Significantly anti-correlated, but positive, BOLD signal changes during respiratory challenges were identified in voxels primarily located near edges of brain spaces containing CSF. These positive BOLD responses occurred earlier than the negative CDB response across most of gray matter voxels. These findings confirm earlier suggestions that in some brain regions, local, fractional changes in CSF volume may overwhelm BOLD-related signal changes, leading to signal anti-correlation. We show that regions with CDB anti-correlated signals coincide with most, but not all, of the regions with negative BOLD signal changes observed during a visual and motor stimulus task. Thus, the addition of a physiological challenge to fMRI experiments can help identify which negative BOLD signals are passive physiological anti-correlations and which may have a putative neuronal origin.

Keywords

fMRI; Negative BOLD; Anti-correlated BOLD; Physiology; Respiratory challenge; Deactivation

Introduction

Blood Oxygenation Level Dependent contrast functional magnetic resonance imaging (BOLD fMRI) takes advantage of the differing magnetic properties of oxygenated and

Published by Elsevier Inc.

[*]Corresponding author at: CUBRIC, School of Psychology, Cardiff University, Cardiff, CF10 3AT, United Kingdom. Fax: +44 29 20 870 339. BrightMG@cardiff.ac.uk (M.G. Bright).

Supplementary data to this article can be found online at http://dx.doi.org/10.1016/j.neuroimage.2013.10.055.

deoxygenated hemoglobin to noninvasively detect neural activity (Bandettini et al., 1992; Kwong et al., 1992; Ogawa et al., 1992). Local increases in neural activity associated with specific brain functions result in simultaneous increases in local blood volume and blood flow to increase oxygen delivery to the active region. To ensure sufficient delivery of oxygen to all tissue (Buxton, 2010), this vascular response ultimately results in decreases in local deoxyhemoglobin concentrations.

Neural activation is therefore linked, via neurovascular coupling mechanisms, to a decrease in [dHb] and thus an increase in BOLD-weighted MR signal (also called “positive” BOLD signal changes). The link between increases in neural activity and increases in the BOLD signal is well-studied and forms the basis for data interpretation in the majority of existing fMRI research and applications, although more research is needed to fully understand how the neural-physiological mechanisms are affected by disease, age, or other factors (Buxton, 2012).

In contrast, the analysis and interpretation of decreases in BOLD signal (also called “negative BOLD” signal changes) is less well developed. For example, signal decreases in BOLD-weighted fMRI have been interpreted as neuronal deactivation (Shmuel et al., 2006), a vascular steal phenomenon (Harel et al., 2002), or a by-product inherent to data processing and analysis techniques (Murphy et al., 2009). Recently, a highly averaged and low-noise fMRI data set consisting of 100 runs per subject identified task-based modulations throughout most of the brain, with 68% of the brain exhibiting “non-conventional” BOLD responses, including negative signal changes (Gonzalez-Castillo et al., 2012). These responses could not be modeled using the standard block or event-related stimulus models of activation. Developing a better understanding of mechanisms underlying negative BOLD signals could therefore have implications for how we collect and interpret fMRI data.

A recent study reported negative fMRI signal changes in large pial and ependymal veins near sulcal and ventricular cerebrospinal fluid (CSF), fluctuating in sync with low-frequency resting state fluctuations (Bianciardi et al., 2011). Data modeling suggested that these negative signals did not originate from local increases in [dHb] but rather local increases in cerebral blood volume (CBV)in voxels with large CSF content. If disproportionally large, such signals can locally overwhelm any positive BOLD effect.

Negative BOLD responses have also been observed in response to physiological challenges such as manipulations of arterial CO_2 gas content. Although most of the brain demonstrates a positive BOLD signal change associated with the vasodilatory effects of hypercapnia, negative BOLD signal changes have been observed in white matter regions (Mandell et al., 2008) and in ventricles (Blockley et al., 2011) of healthy individuals. Although these studies do not give evidence that negative reactivity to increased CO_2 is related to the negative BOLD signals observed by Bianciardi et al. in resting state data, they suggest that respiratory challenges may offer a method for probing the negative BOLD phenomenon.

In the current study, we further investigated the origin of negative BOLD signals by applying a Cued Deep Breathing (CDB) task (Bright et al., 2009) that uses two cycles of short, deep breaths to create transient hypocapnia and a resultant global fMRI signal

decrease caused by constriction of vascular smooth muscle, primarily in cerebral arterioles (Brian, 1998). We hypothesized that a global stimulus will amplify the effect in large vessels and that using a global negative stimulus will test whether these voxels exhibit negative or simply anti-correlated responses. Furthermore, we hypothesized that analysis of the relative timing of the positive and negative fMRI signal changes may give better insight into the underlying mechanisms. Finally, we analyzed fMRI signals acquired during visual and motor stimuli, and compared the location and response dynamics of positive and negative signals of neural and hemodynamic challenges.

Methods

Data acquisition

Ten subjects (aged 23–56 years, mean age = 36 years, 3 females) were scanned using a 7 Tesla GE whole-body MRI scanner (Milwaukee, WI, USA) with a 32-channel receive head coil. Data were acquired using a BOLD-weighted gradient-echo echo-planar imaging (EPI) sequence (TR/TE = 2000/30 ms, FOV = 260 mm, flip angle = 67°, slice thickness = 2 mm with 0.2 mm gap, 2.0 × 2.0 × 2.0 mm^3 resolution). Twenty oblique slices were acquired in an interleaved fashion to cover both motor and visual cortices. The EPI read-out occurred during the first 1500 ms of each TR period, creating 500 ms breaks in the scanner noise for delivery of auditory commands. One whole-brain EPI data set was also acquired to facilitate the creation of CSF masks (55 slices at identical oblique angle and using otherwise identical scan parameters as the functional data).

In the Breathing scan, subjects were instructed to execute 6 CDB challenges interleaved with 75 s of normal breathing using spoken auditory commands (“Ready”, “In”, “Out”, “In”, “Out”, “Normal”) via the scanner intercom system. Cued instructions were shortened from the original instructions (Bright et al., 2009) to improve clarity in the limited acoustic gaps. Subjects were asked to keep their eyes closed and auditory commands were used to limit confounding neural activation in the visual cortex, one of the areas targeted with other tasks in our study. The total scan duration was 8.5 min (255 repetitions), and 9 of the 10 subjects performed a second, identical repeat of this scan.

In the VisualMotor scan, subjects were presented with a flashing checkerboard visual stimulus (7.5 Hz, full contrast) delivered in a rapid, pseudo-random manner using a binary m-sequence paradigm. The m-sequence was chosen because of its (virtually) zero-autocorrelation property, allowing extraction of the hemodynamic response function (HRF) on a voxel-by-voxel basis (i.e. voxel-wise) with high efficiency (Kellman et al., 2003). A 127 bin m-sequence with inverse-repeat was used, both padded to 150 bins yielding a total of 300 bins (2-s bin duration, total scan duration = 10 min). Each subject was asked to repeatedly press a button when the flashing checkerboard was displayed to effectuate concurrent visual and motor stimulation.

Finally, a visual and motor functional Localizer scan was acquired using a block design flashing checkerboard paradigm (30 s off, 30 s on, 5 repetitions), and the subject was asked to repeatedly press the button with their finger during the “on” blocks.

Subjects were fitted with respiratory bellows to monitor depth and rate of breathing; these data were also used to monitor compliance with the breathing task and to reduce respiration-driven scanning artifacts using real-time shimming (van Gelderen et al., 2007). As most of the effects of respiration on B_0 are linear with chest position, we assume that the real-time shimming algorithm, although optimized for normal breathing, will correct much of the artifacts associated with the CDB challenges in addition to resting respiration.

Data analysis

In preprocessing, the first 9 volumes of the Breathing and VisualMotor data were removed, motion correction (MCFLIRT, FSL, FMRIB, University of Oxford, UK), brain extraction (BET, FSL), and slice timing correction (FSL) were performed, and a 4-degree polynomial detrending was applied (IDL, Exelis Visual Information Solutions, Boulder, CO USA). Temporal ICA (MELODIC) was then performed, and components identified to contain severe motion-related artifacts were removed from the data. The criteria for removing a component were as follows: the time series contained 1–3 signal spikes of at least 7% signal change (larger than most physiologically derived BOLD signal changes), and the associated spatial map featured 1–4 slices in an interleaved pattern. (The interleaved characteristic results from the interleaved acquisition of the slices.) These criteria removed the largest head motion artifacts but did not exclude the head motion associated with all of the 6 CDB challenges.

The Localizer data were analyzed using a general linear model: the block design paradigm was convolved with a canonical hemodynamic response function and a mask of significantly activated voxels (conservative threshold at $Z > 5.0$) was extracted for each subject. The block design was utilized to more accurately identify active voxels; assuming that a correct impulse-response function is used, a conventional block paradigm has increased detection power as a single metric (activation amplitude) is derived. It is less straightforward to extract a single significance measure from the m-sequence data, where the response amplitude at various latencies is measured. No clustering algorithm was applied, as individual voxel behavior was of interest.

Correlation analysis

Negatively activating voxels were identified from correlation analysis with a reference time series, created for each Breathing and VisualMotor data set. Because we are using a global physiological stimulus in the Breathing scan, the global time series (mean signal in the brain over time) was used as the reference time series in the Breathing data. Note that the global signal was not used as a regressor, as this can create artificial anti-correlations (Murphy et al., 2009). The reference time series was extracted from the data rather than constructed using a model of the breathing stimulus in order to account for variability in CDB task execution and the physiological response across subjects. For the VisualMotor data, we averaged the voxel time series within the activation mask obtained from the Localizer data set to create a reference time series. In the Breathing data, we compared the global time series with the time series averaged across the activation mask: the correlation between these time series was calculated for each subject and transformed into z(r) values using the Fisher transform. The mean z(r) averaged across subjects was 1.87 ± 0.39, and the median r value

across subjects was 0.97, demonstrating that voxels within the activation mask behave similarly to voxels throughout the brain.

The correlation coefficient between the reference time series and every individual voxel time series was calculated for both data sets, and significantly correlated or anti-correlated voxels ($p < 0.05$, Bonferroni corrected) were identified. The spatial distribution of voxels showing significant anti-correlations in the Breathing and VisualMotor data sets were compared: maps identifying overlapping and non-overlapping voxel populations were extracted.

Estimation of the voxel-wise hemodynamic response functions

The voxel-wise BOLD response to the breathing challenges and visual/motor stimulus was extracted from the data.

In the Breathing data, the start of each CDB challenge was determined using the respiratory bellows data (temporal resolution = 0.05 s). A trial-specific temporal shift was calculated from the offset of the start of the deep breaths to the nearest fMRI volume acquisition. For each voxel, the fMRI data for each of the six challenges were combined into one time series, using the trial-specific shifts for greater accuracy (Fig. 1). The combined data were fitted with a double gamma-variate function (MATLAB, Mathworks, Natick, MA USA) and interpolated to a resolution of 0.25 s. This fitted response to the respiratory challenges is referred to as HRF_{resp}.

In the VisualMotor data, the m-sequence paradigm was deconvolved from the voxel-wise time series data using correlation analysis as was described earlier (Kellman et al., 2003), and the resulting voxel-wise HRFs with 2-s resolution were interpolated using splines to a temporal resolution of 0.25 s. This deconvolved response to the visual and motor stimulus is referred to as HRF_{vm}.

Response timing analysis

The dynamics of the anti-correlated and correlated BOLD responses were compared in two ways. First, the voxel-wise hemodynamic response function was averaged over the significantly correlated and anti-correlated voxels, and the time to (absolute) peak (TTP) values of the averaged HRF_{resp} and HRF_{vm} were identified. (Note that the absolute “peak” of the response identifies the extremum of a negative BOLD signal change in both the correlated Breathing and the anti-correlated VisualMotor data).

As both the response amplitude and TTP in larger draining vessels increase together, this would potentially create a confound in the averaged HRF. To remove this confound, the TTP of every voxel HRF was identified and the median TTP value within significantly correlated and anti-correlated voxels was calculated. Voxels that exhibited extremely early TTP values (signal changes during the stimulus or task that are likely to be artifactual) were not included in these calculations: TTP values earlier than 8 s in the Breathing data and earlier than 1.5 s in the VisualMotor data were eliminated (The numbers of voxels remaining following this thresholding are provided in Table 1b). For both analyses, these TTP values were compared across subjects using paired t-tests with a significant threshold of $p < 0.05$.

Results

Three subjects (1, 3, and 9) were excluded due to errors in collecting physiological data or poor task performance. In one of the 7 remaining subjects, only a single repeat of the Breathing scan was available, rather than two repeats for all other subjects (denoted as $Breathing_1$ and $Breathing_2$).

Correlation analysis

The numbers of voxels significantly correlated or anti-correlated with the reference time series for each data set are given in Table 1a. Significant anti-correlation was observed in all data sets, with large inter-subject variability in the spatial extent of these effects. This variability may reflect inherent differences in subject physiology, task execution, or image slice positioning. In all data sets, fewer voxels exhibited significant anti-correlation than correlation with the reference time series ($p < 1.0 \times 10^{-4}$, paired *t*-test, corrected for multiple comparisons). The VisualMotor data showed fewer significantly correlated voxels than the Breathing data sets ($p < 0.005$), which likely reflects the more local nature of the VisualMotor task compared to the global hypocapnia challenge in the Breathing data. However, the percentage of anti-correlated voxels relative to correlated voxels was larger (~10%) in the VisualMotor data than in the Breathing data (~4.5%). No significant difference was observed between the numbers of correlated and anti-correlated voxels across the two Breathing scans, indicating general reproducibility of the correlation effects.

Fig. 2a shows examples of the reference time series and unthresholded correlation maps for one subject. The BOLD response to the six CDB challenges is clearly visible in the reference time series of the Breathing data, while the response to the pseudo-random m-sequence stimulus in the VisualMotor data is not directly interpretable. Fig. 2b illustrates the time series of individual voxels in the $Breathing_1$ data set, giving examples of the correlated and anti-correlated BOLD signals. The mean time series across significantly correlated and anti-correlated voxel populations for both the VisualMotor and $Breathing_1$ data sets of all subjects are provided in the Supplementary Fig.

The thresholded correlation maps for all subjects are shown in Fig. 3. In the Breathing data, anti-correlations (shown in red) are primarily observed in voxels along the edges of ventricles, which is consistent with the previous study (Bianciardi et al., 2011). Additional voxels near the pial surface of the brain, as well as within white matter, also demonstrate significant anti-correlation.

To better understand the spatial localization of these anti-correlated voxels, masks defining the edges of CSF were created for each subject. CSF voxels were identified in the whole-brain EPI data set using FMRIB's Automated Segmentation Tool (FAST, FSL) (Zhang et al., 2001), and this mask was eroded, dilated, or dilated twice. The number of significantly anti-correlated voxels present within the original CSF mask and each of these manipulated masks was counted. The results are presented in Fig. 4, as percentages of the total number of anti-correlated voxels in the brain for each subject. Approximately 80–90% of significantly anti-correlated voxels are located near the boundary of CSF regions.

The VisualMotor correlation maps show significant correlations beyond the expected activation areas (motor and visual areas); because physiological noise was not removed in this study (physiological fluctuations are the effect of interest in the Breathing data), the effects of cardiac pulsation and respiration are still present in the data and may cause additional correlations unrelated to the stimulus, albeit this is unlikely to be a large effect for the pseudo-random m-sequence paradigm. Additional networks related to attention may also have been involved in performing the task. In several subjects, the VisualMotor data exhibited significant anti-correlation in voxels near the edges of ventricles, in good agreement with the Breathing results (e.g., Subjects 2, 6, 7, and 8 in Fig. 3). The mask of the significant anti-correlations in the $Breathing_1$ data set for each subject was dilated by one voxel (to account for minor mis-registration between data sets), and the overlap of the VisualMotor and the $Breathing_1$ anti-correlations was determined (Fig. 5). In the VisualMotor data, 66 ± 12% of significantly anti-correlated voxels overlapped with the dilated $Breathing_1$ anti-correlation mask.

Timing analysis

The voxelwise Breathing data was fit with a double gamma-variate function as described in the methods. This function was used by Birn et al. to fit the BOLD response to a single breath (Birn et al., 2008), and by extending the range of allowed parameter values we were able to successfully fit the BOLD response to the two deep breaths in the CDB challenge. Inter-subject variation in the BOLD response was sufficiently accounted for in the fitting: example fits of the global time series for each subject are shown in Fig. 6. This fitting technique has been previously applied in BOLD data acquired at 7 Tesla (Bright et al., 2011) and robustly mapped the regional heterogeneity in CDB response dynamics first observed using averaging and interpolation analyses (Bright et al., 2009).

The average percentage fit error across the 6 CDB trials was calculated, and the median errors across the significantly correlated and significantly anti-correlated voxel populations were determined. The group results are presented in Fig. 6. Fitting errors may reflect insufficient modeling of the BOLD response with the double gamma-variate function, but these results suggest that inter-trial variation in the CDB task and response is a greater influence. The mean error values within 5-TR and 10-TR windows centered approximately on the signal peak were not significantly different in the correlated and anti-correlated voxels (paired *t*-test across subjects, $p > 0.05$), indicating that data from both voxel populations were similarly well fit by the analysis.

Average HRFs

The fitted or deconvolved BOLD signal responses, averaged across voxels that were identified as being significantly correlated (or anti-correlated) with the reference time series, were calculated for each data set. Average HRF_{resp} and HRF_{vm} results are shown in Fig. 7 (in the Breathing results, the data from the scan with the greatest number of significantly anti-correlated voxels, as determined using Table 1, are shown).

The TTPs of the averaged HRFs were determined (Table 2, and indicated using dashed lines in Fig. 7). The TTP of the average anti-correlated HRF_{resp} occurred significantly earlier than

the TTP of the average correlated HRF_{resp} in the $Breathing_1$ data ($p = 0.008$, paired *t*-test, corrected for multiple comparisons). The $Breathing_2$ scan showed similar group results to the $Breathing_1$ scan, but the difference in response TTP did not reach significance, potentially due to fewer subjects being included. (When the $Breathing_1$ and $Breathing_2$ results for each subject were averaged together, the difference between the correlated and anti-correlated TTP was significant; $p = 0.02$, paired *t*-test, corrected for multiple comparisons). There was no significant difference in the timing of the average HRF_{vm} of correlated voxels and the average HRF_{vm} of anti-correlated voxels in the VisualMotor data.

Voxel-wise HRFs

Because the average HRF_{resp} and average HRF_{vm} could be confounded by interaction between the amplitude and timing of the BOLD response, the median TTP of significantly correlated/anti-correlated voxels was also determined (Table 2). The median TTP, which is more immune to outliers than the mean, was significantly earlier in the anti-correlated voxels relative to the correlated voxels in the $Breathing_1$ and $Breathing_2$ data sets ($p = 0.008$ and $p = 0.02$, respectively; paired t-test, corrected for multiple comparisons), in agreement with the average HRF_{resp} analysis. To show this shift graphically, histograms of the TTPs of the Breathing data are presented in Fig. 7. Again, there was no significant difference in the VisualMotor data.

Finally, additional timing analysis was performed in light of the clustered anti-correlations observed in the VisualMotor data sets of three subjects, ipsilateral to the hand involved with the motor task (right-hand side of Fig. 5) that did not show an overlap with the Breathing data anti-correlations. In three subjects (5, 6, and 7), regions of interest were manually drawn to include activation associated with the motor task and a similar region in the opposite hemisphere (inserts in Fig. 8). Two populations of voxels were compared: voxels that showed significant activation in the Localizer scan located approximately near the motor cortex contralateral to the active hand, and voxels that exhibited significant "unexplained" anti-correlations in the ipsilateral cortical areas. Histograms of the TTPs of these voxel groups are presented in Fig. 8. The "unexplained" anti-correlations in the area ipsilateral to hand activity are slightly delayed with respect to the correlated (activated) voxels.

Discussion

We successfully mapped significant anti-correlations in BOLD fMRI data during physiological and neural stimulus paradigms. Our results enable us to draw three principal conclusions.

Anti-correlated signal changes are not inherently negative

Firstly, we showed that anti-correlated BOLD signal changes preferentially occur near the edges of ventricles and at the surface of the brain, in contrast with brain regions whose signal positively correlates with the reference region. This is most apparent in the Breathing data sets, where the global BOLD signal decreases due to mild hypocapnia challenges, and the BOLD response in the anti-correlated voxels is positive. Thus, although in some cases

this phenomenon may appear as a “negative BOLD” signal change, the polarity of the response is actually determined by the surrounding signal changes.

BOLD anti-correlations are inherent to physiological response

Secondly, this anti-correlated phenomenon does not require neuronal de-activation, because we observe it in the BOLD response to Cued Deep Breathing challenges. This indicates that it is a vascular phenomenon inherent to the BOLD response itself, rather than reflecting a neuronal deactivation. This could not be concluded in an earlier work (Bianciardi et al., 2011), where resting state low-frequency oscillations were used as the “stimulus” or reference for mapping anti-correlations: these resting oscillations are, at least to some degree, neuro-metabolic in origin (Fukunaga et al., 2008; Leopold and Maier, 2012). There is neural activity associated with any controlled respiratory challenge, including the CDB challenge, however these effects are typically localized to the insula and deep gray matter structures (McKay et al., 2003) and not to pial or periventricular vessels. There may also be arousal effects associated with hypocapnia; hypercapnia (elevated CO_2 levels) has been shown to decrease resting neural activity (Hall et al., 2011; Zappe et al., 2008), and thus the hypocapnic CDB challenge may result in temporary changes in baseline activity. Further research is needed to determine how these effects influence the BOLD reactivity response timing in the voxel populations examined in the current study.

Also, the BOLD response to CDB challenges peaks at approximately 19.6 s following the start of the challenge ((Bright et al., 2009), in agreement with the current study). The anti-correlated HRF_{resp} peaks at approximately 18.5 s (Table 2). Because the CDB challenge involves 8 s of deep breaths, this equates to approximately 10.5 s following completion of the respiratory task. In contrast, the BOLD response associated with event-related neural activity peaks at approximately 4–6 s following activation (HRF_{vm} TTP results in Table 2 and Fig. 7; (de Zwart et al., 2009)). This is further evidence that the anti-correlated response is not reflective of neural activity associated with the act of performing CDB challenges.

Mechanism of early physiological BOLD anti-correlations

Finally, our calculations show that the anti-correlated response reaches its peak significantly earlier than the correlated response throughout gray matter in the Breathing data, and occurs mostly in voxels near the edges of CSF. This supports the hypothesis and modeling results of Bianciardi et al. (2011) that the anti-correlations reflect changes in the relative size of the blood and CSF compartments in voxels dominated by these two signal sources: using an m-sequence stimulus paradigm in rats, the iron oxide blood volume impulse response has been observed to peak significantly earlier than the BOLD impulse response (Silva et al., 2007).

The BOLD signal is described by an exponential decay, $S = S_0 e^{-t\,R2^*}$, where R_2^* is dependent on the local concentration of deoxyhemoglobin, [dHb] (Boxerman et al., 1995), and S_0 is related to tissue proton density and T_1. To increase the measured signal S and result in the anti-correlated response in the Breathing data, either [dHb] must decrease, reducing the R_2^* decay constant locally, or S_0 must increase.

One method for decreasing [dHb] is an increase in blood flow that enhances the “wash out” of deoxyhemoglobin. Our results show that this “flow-related” mechanism is not the primary

mechanism underlying the observed BOLD anti-correlations. The hypocapnic CDB challenge used in this study causes global vasoconstriction (which is regulated primarily at the arteriolar level), and thus decreases blood flow throughout the brain and increases [dHb] in the tissue. Still, it is likely that we are observing anti-correlations near large veins (Bianciardi et al., 2011), which may not exhibit the same relative [dHb] changes as the bulk of gray matter. However, we also observe that the anti-correlated BOLD signal in these large draining vessels occurs earlier than the “upstream” global BOLD signal in the Breathing data, indicating that sluggish, flow-related [dHb] effects are not the source of the observed anti-correlated signal changes.

Alternative mechanisms for producing the anti-correlated signals in the Breathing data are volume-related: decreases in [dHb] linked to vasoconstrictive reductions in blood volume and/or increases in S_0 associated with changes in the relative volume of signal compartments within a voxel. As already discussed, local blood volume is decreased on the arterial side of the vascular tree due to the hypocapnic CDB challenge, and this could be linked to passive venous vessel constriction in the context of reduced perfusion pressure and a balloon model of venous compliance (Buxton et al., 1998). This, however, does not explain the spatial distribution of the anti-correlated voxels. The localization of the anti-correlated response to voxels in large veins proximal to CSF stores (e.g., at the edge of ventricles or on the surface of the brain) indicates that changes in the relative volume of both the blood and CSF compartments are critical in developing the anti-correlated signals.

This explanation is in agreement with the existing literature. The Monroe–Kellie doctrine states that changes in blood volume must be balanced by appropriate changes in other compartment volumes to maintain stable intracranial pressure (Mokri, 2001). The widespread reduction in arterial blood volume in our data (associated with the vasoconstrictive hypocapnia challenges) must therefore be linked to a matching increase in CSF volume. Voxels containing large CSF contributions (although not located entirely within CSF) reflect this shift: increases in the CSF compartment will increase the proton density and the apparent T_1 within a given voxel, and thus S_0. This change in CSF volume linked to changes in blood volume has been observed throughout the brain by fitting multi-echo data to a multi-compartment model (Piechnik et al., 2009). In our data, we observe that the S_0 effect is overwhelmed by the flow-related [dHb] effect in most of the brain, except in certain voxels where the CSF compartment may have both greater initial volume and ability to increase in volume as ventricle edges are pushed outwards or surface veins are compressed. This S_0 effect may be bolstered by an R_2* effect: the R_2* of CSF is smaller than that of gray matter, and thus blood volume changes will be associated with greater BOLD contrast when in the proximity of CSF compared to within gray matter, potentially overwhelming any flow-related [dHb] effects.

To summarize, the early response timing of the BOLD anti-correlations observed in the Breathing data indicates flow-related [dHb] mechanisms are not responsible. The localization of the anti-correlations to voxels with large blood/CSF volumes supports a volume-related S_0 mechanism, although changes in [dHb] linked to blood volume changes likely also contribute.

Differences in BOLD anti-correlations in Breathing and VisualMotor data sets

As shown by the substantial overlap of the anti-correlated signal ROIs for both tasks (Fig. 5), the VisualMotor data exhibited significant BOLD anti-correlations in many of the same voxels as the Breathing data. These overlapping voxels are located at the edges of ventricles and at points on the surface of the brain, as well as other less well-defined locations, primarily near the edges of CSF. We attest that this overlap demonstrates the shared mechanisms of certain BOLD anti-correlations in these data sets: the VisualMotor data is associated with a widespread increase in blood volume, which is matched by a corresponding decrease in relative CSF volume and S_0 in certain voxels. The overlap of the observed anti-correlations can therefore be explained by the physiological mechanisms described above.

There also exist several non-overlapping, or “unexplained” anti-correlations in the VisualMotor data. Most interestingly, three subjects demonstrate slightly delayed anti-correlations in (approximately) the somatosensory/motor cortex ipsilateral to the hand involved with the motor task. Although the timing results are difficult to interpret given the small numbers of voxels and insufficient temporal resolution, the findings in Fig. 8 suggest that these “unexplained” BOLD anti-correlations may reflect a neurovascular mechanism of truly “negative” BOLD signal changes with a neuronal basis (e.g., deactivation).

Negative BOLD signals have been observed previously in the somatosensory region ipsilateral to a motor task (Gonzalez-Castillo et al., 2012; Kastrup et al., 2008), and are likely to have a neural origin (Pasley et al., 2007). Additionally, more recent literatures link negative BOLD signals to decreases in blood flow, both in visual cortex during a partial-field visual stimulus (Goense et al., 2012) and in the somatosensory cortex ipsilateral to median nerve stimulation (Schäfer et al., 2012). This suggests that the “unexplained” anti-correlations that we observe (Figs. 6 and 8) have a different, potentially “flow-related” mechanism compared to the anti-correlations also present in the Breathing data, which is supported qualitatively by the different response timing.

These “unexplained” anti-correlated voxels extend beyond the somatosensory and motor cortices in our data. Indeed, although 65% of anti-correlated voxels in the VisualMotor data overlapped with anti-correlated voxels in the Breathing data, this leaves 35% of anti-correlated voxels with potentially different underlying mechanisms responsible for the negative BOLD signal change. Some regions, such as near the edges of visual activation, are expected to show negative BOLD responses during visual stimulation (Shmuel et al., 2006). Interestingly, in our data, there are many anti-correlations near the visual activation area that are present in both Breathing and VisualMotor data sets (e.g., Subject 2 in Fig. 5). We conclude that incorporating a physiological challenge such as Cued Deep Breathing may help to differentiate between voxels with a physiological (pure vascular) anti-correlated BOLD signal change and those showing a true negative BOLD signal change with an underlying neuro-vascular mechanism, particularly in regions where both responses may be present.

Influence of other noise sources

The data sets in this study contain numerous noise sources in addition to the physiological or neural signals of interest. It is important to note that head motion, cardiac pulsations, and other global noise sources could influence the identification of correlated and anti-correlated voxels. In the Breathing data, head motion can be assumed to be extreme and task-locked, making motion artifacts particularly challenging to compensate for. However, during CDB tasks, motion has been observed to occur primarily in the period of the deep breaths, thereby finishing before the actual BOLD signal change of interest (in the window of interest, motion is minimal) (Bright et al., 2009). Still, in both the Breathing and VisualMotor data, more subtle head motion or other widespread noise sources throughout the scan may influence our correlation analysis. These confounds would not, however, influence the polarity of the mean HRF extracted from these voxels or significantly affect the TTP of this response in any systematic manner. The differing polarity of the average HRFs suggests that the influence of global noise on our conclusions is minimal. We recommend that future studies adopt multi-echo acquisitions to better isolate the BOLD signal from noise sources (Bright and Murphy, 2013) and better understand the physiological mechanisms underlying the measured BOLD-weighted data.

Conclusions

We have identified anti-correlated BOLD signal changes in response to respiratory challenges in voxels primarily located near edges of CSF stores. These signal changes occur earlier than the response across most of gray matter voxels. We conclude that these signal changes can be attributed primarily to changes in S_0 associated with increases in intracranial CSF volume during widespread changes in cerebral perfusion. Changes in local [dHb] in these voxels, as CSF displaces the intravascular compartment, may augment this mechanism.

We also show that the physiological BOLD anti-correlations can explain most, but not all, of the negative BOLD signal changes observed in a visual and motor stimulus data set. The negative BOLD signals that are not explained by the respiratory challenge data demonstrate a delayed response timing compared to associated correlated BOLD activations, and are presumably neuronal in origin.

The addition of a physiological challenge to fMRI experiments can help identify which “negative BOLD” signals are passive physiological anti-correlations and which may have a different (e.g., neuronal) origin.

Supplementary Material

Refer to Web version on PubMed Central for supplementary material.

Acknowledgments

We thank Susan Fulton Guttman for her assistance in the data acquisition. This research was supported by the Intramural Research Program of NINDS/NIH and the Wellcome Trust.

References

Bandettini PA, Wong EC, Hinks RS, Tikofsky RS, Hyde JS. Time course EPI of human brain function during task activation. Magn Reson Med. 1992; 25:390–397. [PubMed: 1614324]

Bianciardi M, Fukunaga M, van Gelderen P, de Zwart JA, Duyn JH. Negative BOLD-fMRI signals in large cerebral veins. J Cereb Blood Flow Metab. 2011; 31:401–412. [PubMed: 20859295]

Birn RM, Smith MA, Jones TB, Bandettini PA. The respiration response function: the temporal dynamics of fMRI signal fluctuations related to changes in respiration. NeuroImage. 2008; 40:644–654. [PubMed: 18234517]

Blockley NP, Driver ID, Francis ST, Fisher JA, Gowland PA. An improved method for acquiring cerebrovascular reactivity maps. Magn Reson Med. 2011; 65:1278–1286. [PubMed: 21500256]

Boxerman JL, Hamberg LM, Rosen BR, Weisskoff RM. MR contrast due to intravascular magnetic susceptibility perturbations. Magn Reson Med. 1995; 34:555–566. [PubMed: 8524024]

Brian JE. Carbon dioxide and the cerebral circulation. Anesthesiology. 1998; 88:1365–1386. [PubMed: 9605698]

Bright MG, Murphy K. Removing motion and physiological artifacts from intrinsic BOLD fluctuations using short echo data. NeuroImage. 2013; 64:526–537. [PubMed: 23006803]

Bright MG, Bulte DP, Jezzard P, Duyn JH. Characterization of regional heterogeneity in cerebrovascular reactivity dynamics using novel hypocapnia task and BOLD fMRI. NeuroImage. 2009; 48:166–175. [PubMed: 19450694]

Bright, MG.; Bulte, DP.; Jezzard, P.; Duyn, JH. Characterizing the BOLD response to transient respiratory challenges at 7 Tesla. Presented at the 11th Annual Meeting of the International Society for Magnetic Resonance in Medicine; Montreal, Canada. 2011.

Buxton RB. Interpreting oxygenation-based neuroimaging signals: the importance and the challenge of understanding brain oxygen metabolism. Front Neuroenerg. 2010; 2:8. http://dx.doi.org/10.3389/fnene.2010.00008.

Buxton RB. Dynamic models of BOLD contrast. NeuroImage. 2012; 62:953–961. [PubMed: 22245339]

Buxton RB, Wong EC, Frank LR. Dynamics of blood flow and oxygenation changes during brain activation: the balloon model. Magn Reson Med. 1998; 39:855–864. [PubMed: 9621908]

de Zwart JA, van Gelderen P, Jansma JM, Fukunaga M, Bianciardi M, Duyn JH. Hemodynamic nonlinearities affect BOLD fMRI response timing and amplitude. NeuroImage. 2009; 47:1649–1658. [PubMed: 19520175]

Fukunaga M, Horovitz SG, de Zwart JA, van Gelderen P, Balkin TJ, Braun AR, Duyn JH. Metabolic origin of BOLD signal fluctuations in the absence of stimuli. J Cereb Blood Flow Metab. 2008; 28:1377–1387. [PubMed: 18382468]

Goense J, Merkle H, Logothetis NK. High-resolution fMRI reveals laminar differences in neurovascular coupling between positive and negative bold responses. Neuron. 2012; 76:629–639. [PubMed: 23141073]

Gonzalez-Castillo J, Saad ZS, Handwerker DA, Inati SJ, Brenowitz N, Bandettini PA. Whole-brain, time-locked activation with simple tasks revealed using massive averaging and model-free analysis. Proc Natl Acad Sci U S A. 2012; 109:5487–5492. [PubMed: 22431587]

Hall EL, Driver ID, Croal PL, Francis ST, Gowland PA, Morris PG, Brookes MJ. The effect of hypercapnia on resting and stimulus induced MEG signals. NeuroImage. 2011; 58:1034–1043. [PubMed: 21762783]

Harel N, Lee SP, Nagaoka T, Kim DS, Kim SG. Origin of negative blood oxygenation level-dependent fMRI signals. J Cereb Blood Flow Metab. 2002; 22:908–917. [PubMed: 12172376]

Kastrup A, Baudewig J, Schnaudigel S, Huonker R, Becker L, Sohns JM, Dechent P, Klingner C, Witte OW. Behavioral correlates of negative BOLD signal changes in the primary somatosensory cortex. NeuroImage. 2008; 41:1364–1371. [PubMed: 18495495]

Kellman P, Gelderen PV, de Zwart JA, Duyn JH. Method for functional MRI mapping of nonlinear response. NeuroImage. 2003; 19:190–199. [PubMed: 12781738]

Kwong KK, Belliveau JW, Chesler DA, Goldberg IE, Weisskoff RM, Poncelet BP, Kennedy DN, Hoppel BE, Cohen MS, Turner R. Dynamic magnetic resonance imaging of human brain activity during primary sensory stimulation. Proc Natl Acad Sci. 1992; 89:5675–5679. [PubMed: 1608978]

Leopold DA, Maier A. Ongoing physiological processes in the cerebral cortex. NeuroImage. 2012; 62:2190–2200. [PubMed: 22040739]

Mandell DM, Han JS, Poublanc J, Crawley AP, Kassner A, Fisher JA, Mikulis DJ. Selective reduction of blood flow to white matter during hypercapnia corresponds with leukoaraiosis. Stroke. 2008; 39:1993–1998. [PubMed: 18451357]

McKay LC, Evans KC, Frackowiak RSJ, Corfield DR. Neural correlates of voluntary breathing in humans. J Appl Physiol. 2003; 95:1170–1178. [PubMed: 12754178]

Mokri B. The Monro–Kellie hypothesis: applications in CSF volume depletion. Neurology. 2001; 56:1746–1748. [PubMed: 11425944]

Murphy K, Birn RM, Handwerker DA, Jones TB, Bandettini PA. The impact of global signal regression on resting state correlations: are anti-correlated networks introduced? NeuroImage. 2009; 44:893–905. [PubMed: 18976716]

Ogawa S, Tank DW, Menon R, Ellermann JM, Kim SG, Merkle H, Ugurbil K. Intrinsic signal changes accompanying sensory stimulation: functional brain mapping with magnetic resonance imaging. Proc Natl Acad Sci. 1992; 89:5951–5955. [PubMed: 1631079]

Pasley BN, Inglis BA, Freeman RD. Analysis of oxygen metabolism implies a neural origin for the negative BOLD response in human visual cortex. NeuroImage. 2007; 36:269–276. [PubMed: 17113313]

Piechnik SK, Evans J, Bary LH, Wise RG, Jezzard P. Functional changes in CSF volume estimated using measurement of water T2relaxation. Magn Reson Med. 2009; 61:579–586. [PubMed: 19132756]

Schäfer K, Blankenburg F, Kupers R, Grüner JM, Law I, Lauritzen M, Larsson HBW. Negative BOLD signal changes in ipsilateral primary somatosensory cortex are associated with perfusion decreases and behavioral evidence for functional inhibition. NeuroImage. 2012; 59:3119–3127. [PubMed: 22155327]

Shmuel A, Augath M, Oeltermann A, Logothetis NK. Negative functional MRI response correlates with decreases in neuronal activity in monkey visual area V1. Nat Neurosci. 2006; 9:569–577. [PubMed: 16547508]

Silva AC, Koretsky AP, Duyn JH. Functional MRI impulse response for BOLD and CBV contrast in rat somatosensory cortex. Magn Reson Med. 2007; 57:1110–1118. [PubMed: 17534912]

van Gelderen P, de Zwart JA, Starewicz P, Hinks RS, Duyn JH. Real-time shimming to compensate for respiration-induced B0 fluctuations. Magn Reson Med. 2007; 57:362–368. [PubMed: 17260378]

Zappe AC, Uludag K, Oeltermann A, Ugurbil K, Logothetis NK. The influence of moderate hypercapnia on neural activity in the anesthetized nonhuman primate. Cereb Cortex. 2008; 18:2666–2673. [PubMed: 18326521]

Zhang Y, Brady M, Smith S. Segmentation of brain MR images through a hidden Markov random field model and the expectation-maximization algorithm. IEEE Trans Med Imaging. 2001; 20(1): 45–57. Jan. [PubMed: 11293691]

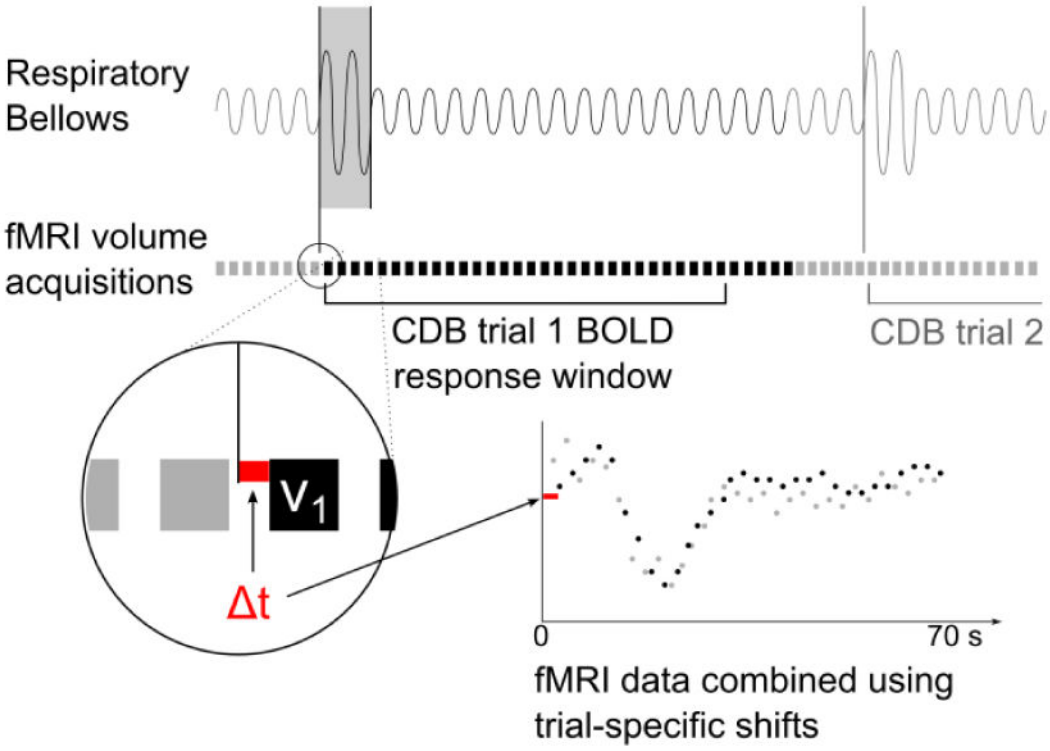

Fig. 1.

Schematic of CDB trial data alignment. The start of each CDB trial was identified in the respiratory bellows data. The closest fMRI volume acquisition was determined (v_1) and a 35-volume window of fMRI data was extracted. The temporal shift between the CDB trial start and the first fMRI volume of that trial was measured (Δt) at a temporal resolution of 0.05 s. The fMRI data from the six CDB trials were combined using these trial-specific temporal shifts, and the combined data were fit using a double gamma-variate function.

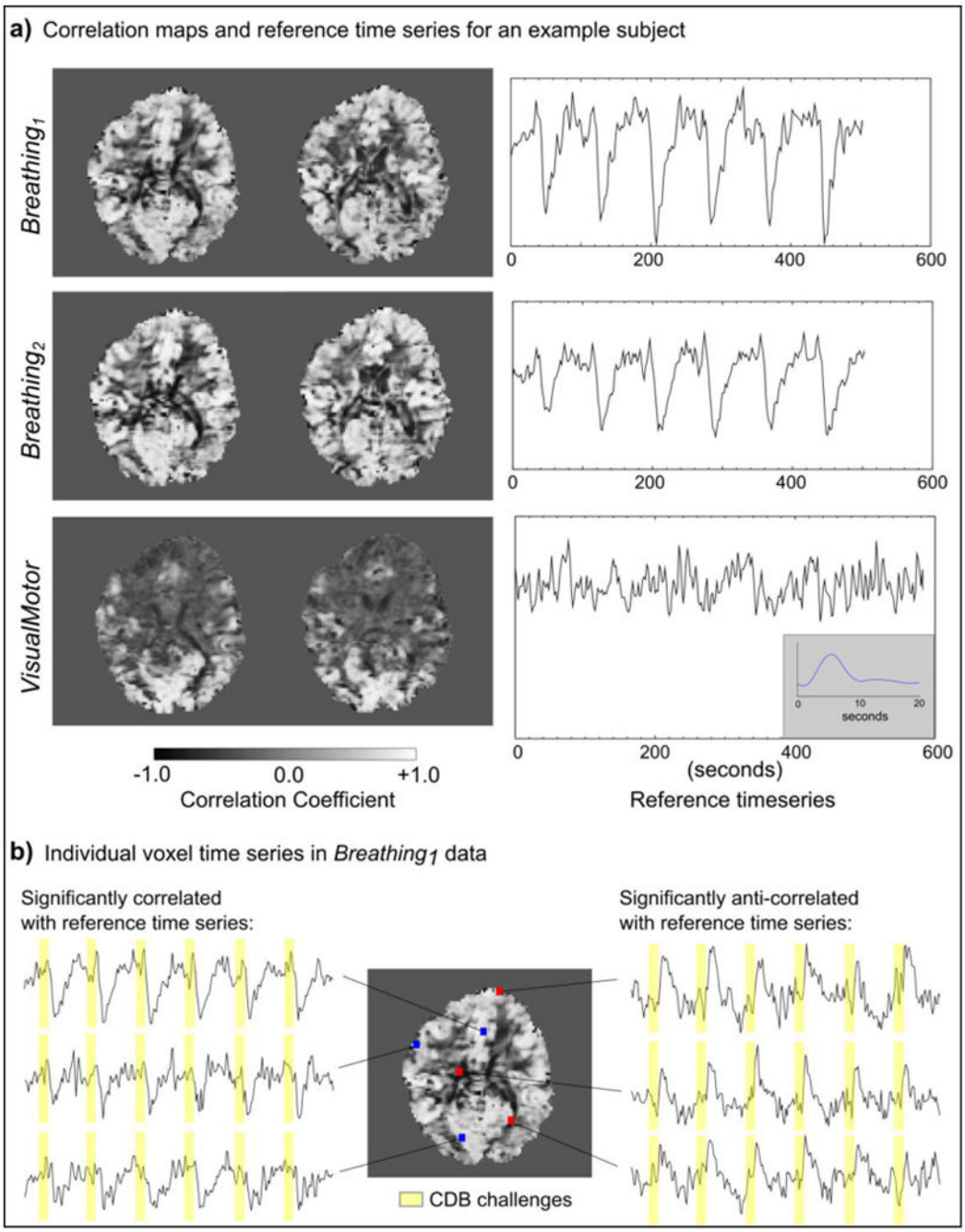

Fig. 2.

Examples of the reference time series for the Breathing and VisualMotor data and voxelwise correlation maps for one subject. In the Breathing data, the global time series was used as a reference. In the VisualMotor data, the average time series within an activation mask (determined by the Localizer scan) was used. The Breathing data showed positive correlation throughout most of gray matter, as well as negative correlations (anti-correlations), most notably at the edges of the ventricles. The VisualMotor data showed less widespread correlations due to the nature of the neural stimulus, but also exhibits anti-correlations in regions similar to those of the Breathing results. The VisualMotor reference time series does not clearly exhibit the m-sequence stimulus paradigm; however, the HRF_{vm} can be extracted from this time series following deconvolution (insert).

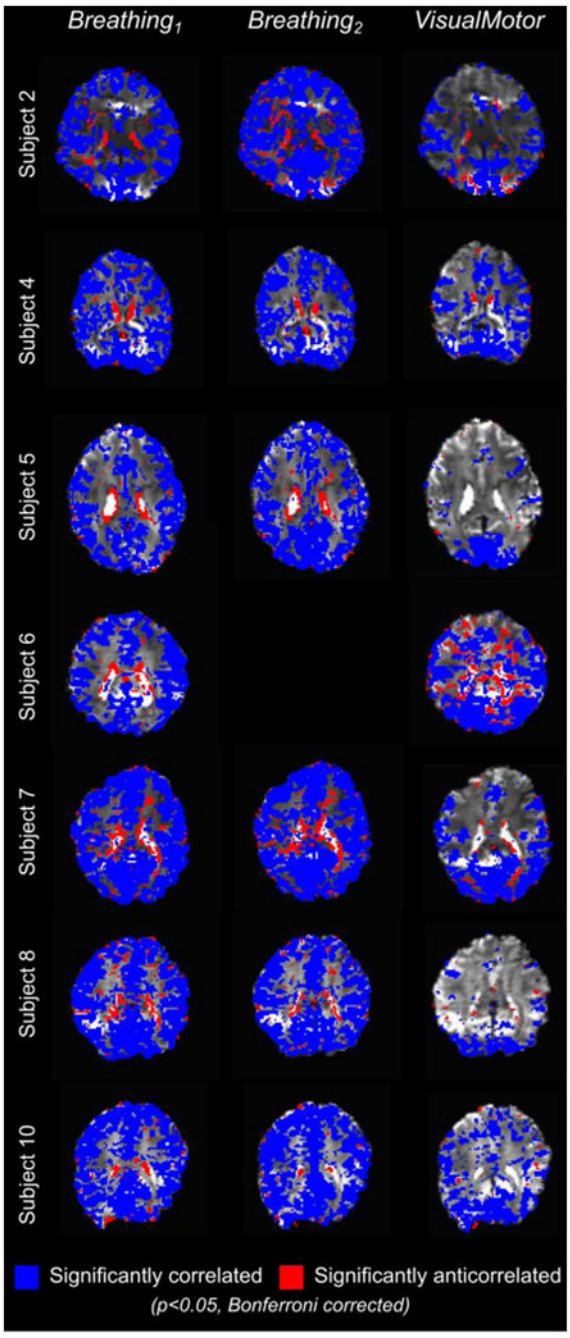

Fig. 3.

Significantly correlated (blue) and anti-correlated (red) voxels in the Breathing and VisualMotor data for all subjects ($p < 0.05$, Bonferroni corrected).

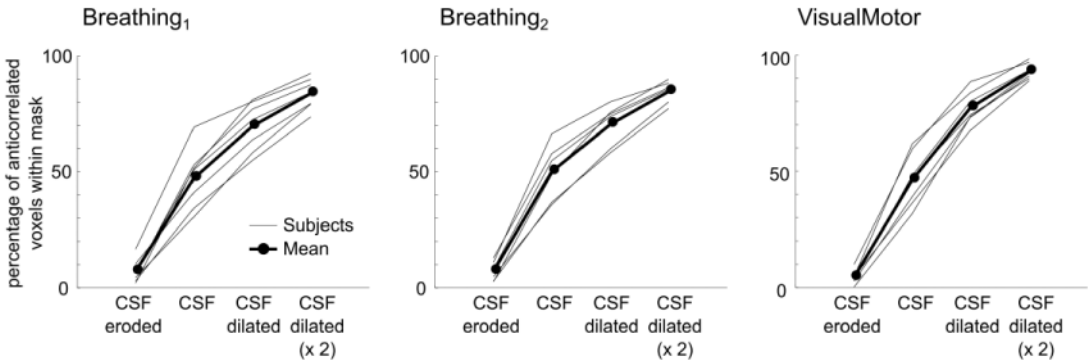

Fig. 4.

Percentage of significantly anti-correlated voxels present within a mask of CSF and the same mask eroded/dilated. Approximately 80–90% of anti-correlated voxels lie near the edges of CSF stores.

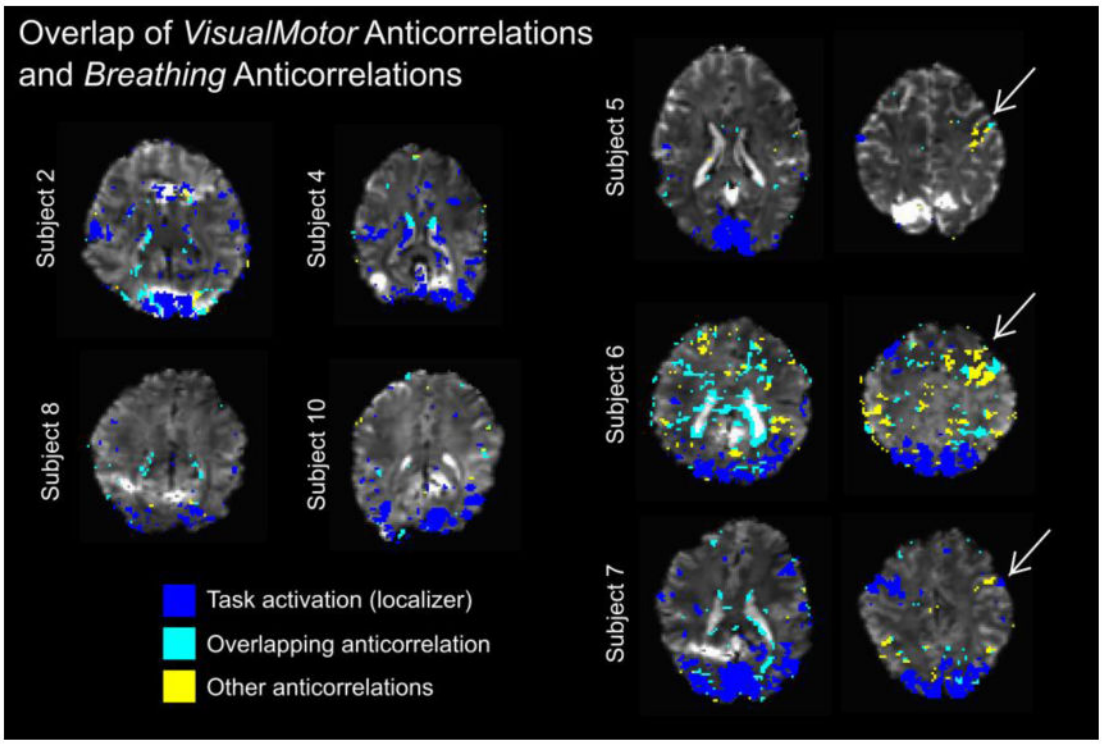

Fig. 5.

Overlap and mismatch of VisualMotor anti-correlations and Breathing anti-correlations. A mask of the significantly anti-correlated voxels in each subject's Breathing data was dilated to account for minor misalignment between datasets. Voxels that were significantly anti-correlated in the VisualMotor data were classified as“overlapping” or“other.” The activation mask from the Localizer scan is included as a reference. Anti-correlations that showed overlap between the two datasets were observed in semi-contiguous groups of voxels (i.e., at the edges of ventricles) as well as more point-like clusters (e.g., near the brain surface). Other (non-overlapping) anti-correlations present in the VisualMotor data were also observed; Subjects 5, 6, and 7 exhibited non-overlapping anti-correlations in areas contralateral to the region of motor activation in the Localizer scan.

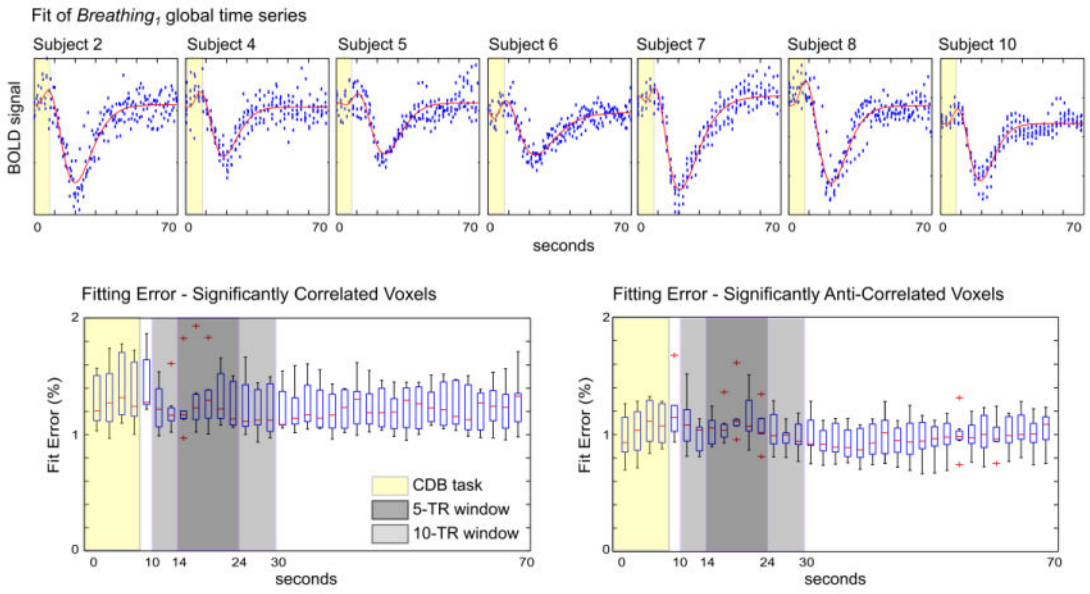

Fig. 6.

Example fit (red lines) of the Breathing$_1$ global time series for each subject (top row). In each voxel time series, the fitting error was averaged across the 6 CDB trials, and the median fitting error of each TR was calculated across the significantly correlated and significantly anti-correlated voxel populations. The results of all subjects are presented (bottom row). There was no significant difference in the mean fitting error of the correlated and anti-correlated data within a 5-TR or 10-TR window encompassing the BOLD signal change of interest.

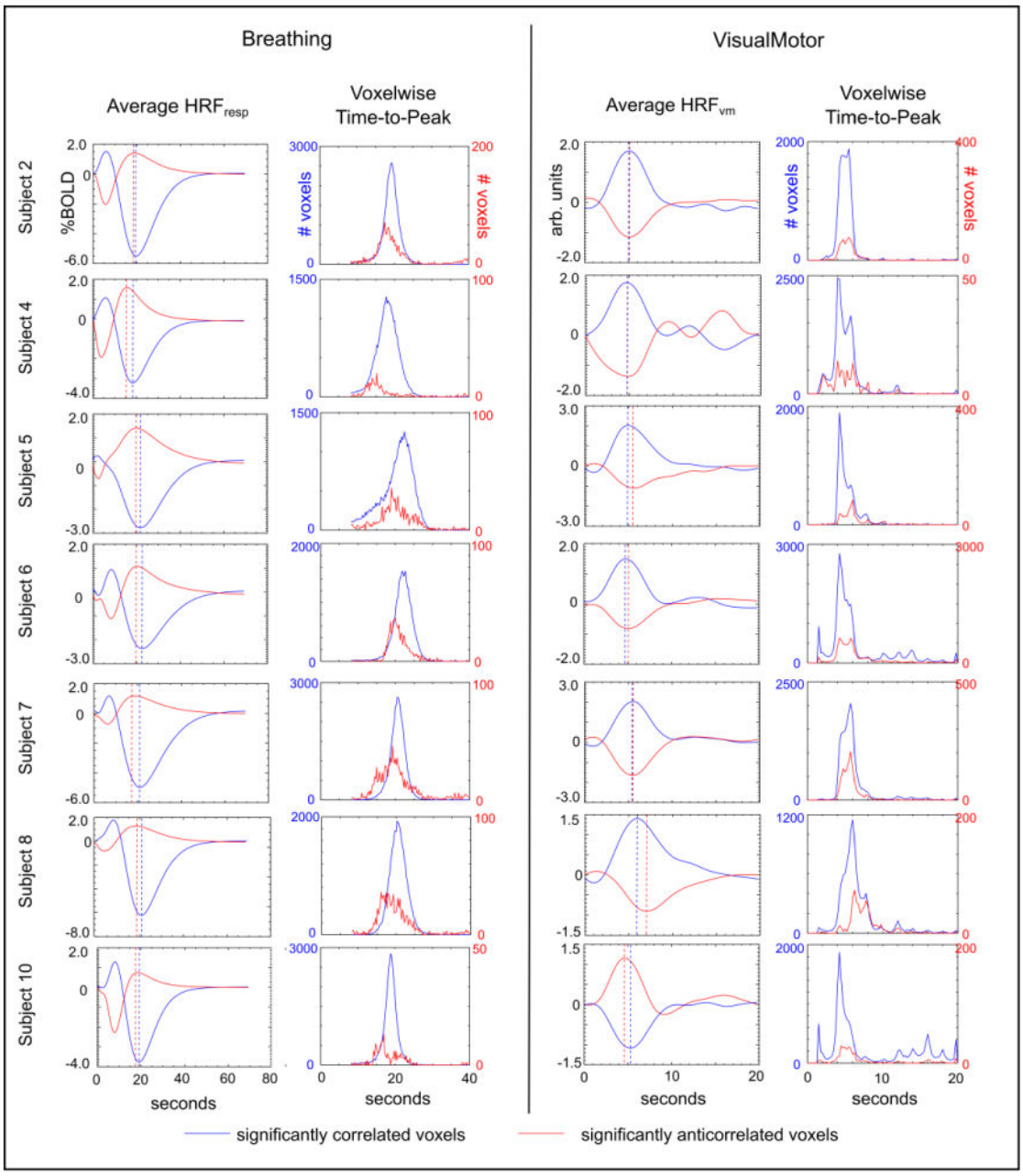

Fig. 7.

Average HRFs (HRF_{resp} and HRF_{vm}) of the significantly correlated/anti-correlated voxels of the Breathing and VisualMotor data sets, and histograms of the TTP values extracted from voxelwise HRFs. The TTPs of the average HRFs are identified (dashed lines). In the Breathing data, the anti-correlated BOLD response appears earlier than the bulk of the correlated response (values are provided in Table 2).

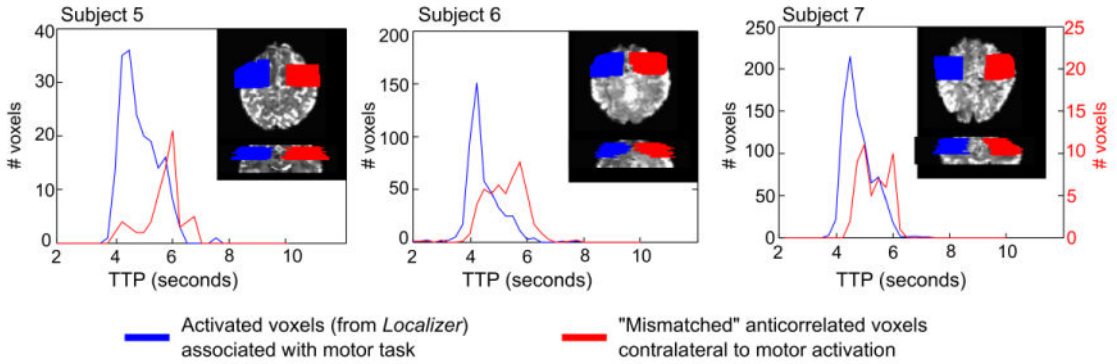

Fig. 8.

Histograms of the time-to-peak (TTP) of the BOLD response in a subset of the VisualMotor data in three subjects identified as having “unexplained” anti-correlations in somatosensory/motor cortical areas (non-overlapping voxels in Fig. 5). Masks were manually drawn to cover the activated (correlated) voxels in the sensorimotor region contralateral to the finger press identified in the Localizer scan. A similar mask in the opposite hemisphere was also drawn, and significantly anti-correlated voxels in this mask (that were not overlapping with anti-correlations in the Breathing data) were identified. The TTP of the anti-correlated BOLD responses (negative BOLD signal changes) in these voxels peaks later than the correlated BOLD response in the activated voxels in the opposite hemisphere.

Table 1

a) Number of voxels significantly correlated or anti-correlated with the reference timeseries ($p < 0.05$, Bonferroni corrected) in the Breathing and VisualMotor datasets. Fewer voxels were identified as significantly correlated in the VisualMotor data relative to the Breathing data (*$p = 0.004$, paired t-tests, corrected for multiple comparisons).

b) Number of voxels significantly correlated or anti-correlated with the reference timeseries that passed TTP thresholding and were included in voxelwise TTP analysis. This thresholding significantly reduced the number of voxels included in the Breathing analysis (**$p < 0.01$, paired-tests, corrected for multiple comparisons).

Subject	$Breathing_1$		$Breathing_2$		VisualMotor	
	Correlated	Anti-correlated	Correlated	Anti-correlated	Correlated	Anti-correlated
a) Number of voxels significantly correlated and anti-correlated with reference time series						
2	39,805	1478	46,379	3679	18,459	874
4	35,605	651	33,569	318	23,175	226
5	40,221	1843	43,256	1912	10,728	626
6	34,484	1597	–	–	26,531	8540
7	46,174	2712	47,712	3005	17,948	1545
8	42,354	2839	40,024	1976	11,213	876
10	40,578	941	39,908	824	19,273	336
Mean	39,889	1723	41,808	1952	18,190	1860
b) Number of voxels remaining after TTP thresholding						
2	38,085	387	44,341	1612	15,925	649
4	32,767	337	31,321	197	21,892	175
5	35,789	622	40,067	928	9483	576
6	32,381	771	–	–	25,367	8163
7	43,804	1065	45,307	1249	17,688	1499
8	40,188	1093	36,966	565	11,050	817
10	38,929	246	37,909	387	18,302	316
Mean	37,420**	646**	39,319**	823	17,101	1742

Table 2

The time-to-peak (TTP) of the average HRF_{resp} and HRF_{vm} in significantly correlated and significantly anti-correlated voxel populations and the associated median voxelwise TTP values. The average HRF_{resp} in anti-correlated voxels exhibited a significantly earlier TTP than the correlated voxels in the $Breathing_1$ data (*p = 0.008), and the median TTP in anti-correlated voxels was significantly earlier than the median TTP of correlated voxels in both the $Breathing_1$ and $Breathing_2$ datasets (*p = 0.008, **p = 0.02, paired t-tests, corrected for multiple comparisons). No significant differences were observed in the VisualMotor data.

Subject	$Breathing_1$		$Breathing_2$		VisualMotor	
	Correlated	Anti-correlated	Correlated	Anti-correlated	Correlated	Anti-correlated
Time-to-Peak of averaged HRF (seconds)						
2	19.50	19.00	19.50	18.75	5.00	5.00
4	18.50	15.75	19.00	17.50	4.75	5.00
5	23.50	21.50	22.00	20.00	5.00	5.75
6	22.75	20.50	–	–	4.75	5.00
7	20.75	18.50	21.00	18.75	5.50	5.50
8	21.00	19.00	21.75	20.75	6.00	7.00
10	19.25	18.75	17.75	18.00	4.50	5.25
Mean	20.75	19.00*	20.17	18.96	5.07	5.50
Median Time-to-Peak of voxels (seconds)						
2	19.00	18.50	19.25	18.25	5.00	5.25
4	18.00	15.00	18.50	17.25	4.75	5.25
5	22.75	22.00	21.25	19.75	5.00	6.00
6	22.25	20.50	–	–	5.00	5.50
7	20.25	19.00	20.75	19.50	5.50	5.50
8	20.50	18.75	21.00	19.25	6.00	7.25
10	18.75	17.00	17.25	17.25	5.50	5.50
Mean	20.21	18.68*	19.67	18.54**	5.25	5.75